Convex Error Growth Patterns in a Global Weather Model

John Harlim,* Michael Oczkowski,† James A. Yorke, Eugenia Kalnay, and Brian R. Hunt
Institute for Physical Science and Technology, University of Maryland, College Park, Maryland 20742, USA
(Received 11 October 2004; published 10 June 2005)

We investigate the error growth, that is, the growth in the distance E between two typical solutions of a weather model. Typically E grows until it reaches a saturation value E_s. We find two distinct broad log-linear regimes, one for E below 2% of E_s and the other for E above. In each, $\log(E/E_s)$ grows as if satisfying a linear differential equation. When plotting $d\log(E)/dt$ vs $\log(E)$, the graph is convex. We argue this behavior is quite different from other dynamics problems with saturation values, which yield concave graphs.

DOI: 10.1103/PhysRevLett.94.228501 PACS numbers: 92.60.Wc, 05.45.Jn, 05.45.Pq

The main characteristic of a temporal chaotic dynamical system is having a positive leading Lyapunov exponent. This quantity measures the long time average exponential growth rate of two solutions initially separated by an infinitesimal distance. One simple example of a chaotic system is the logistic map: $x_{n+1} = 4x_n(1 - x_n)$ with a Lyapunov exponent equal to $\log(2)$. This quantity suggests that the difference between two nearby solutions doubles on each iterate until it reaches saturation. From the point of view of weather forecasting, the logistic map has an infinite limit of predictability: we can always extend the forecast for one iterate by halving the uncertainty of the initial conditions. Lorenz [1] suggested that the Lyapunov exponents may be unbounded for the partial differential equation representing a global atmospheric model. He also argued that at the latest stages the error growth rate behaves differently from Lyapunov exponents.

The atmosphere includes multiple scales of motions, which suggests that different scales of motion grow with different rates. In [2], Lorenz observed that small scales tend to grow at a fast rate and the larger scales of motion grow with a slower rate. He concluded that as one refines the accuracy of the initial states, smaller increments of forecast skill are obtained, and there appears to be a finite limit of predictability. Numerous studies have been devoted to predictability of different types of motion that mimic the atmosphere. For example, Aurell *et al.* [3] shows that in the case of turbulence the growth rate is determined by the cumulative effects of multiple characteristic times.

A hallmark of chaos is the exponential growth of errors, where by *error* we mean the distance $E(t)$ between two trajectories that are close to each other at time $t = 0$. When trajectories are bounded, the exponential growth of $E(t)$ cannot continue indefinitely; $E(t)$ saturates near a value E_s that is representative of the size of the chaotic attractor. We consider the dependence of the exponential growth rate of the error on the size of $E(t)/E_s$ for a global weather forecast model, and we contrast our results with those for some simpler models. The *exponential growth rate* is E'/E where E' is either the time derivative of E or a finite-time approximation of the time derivative. Throughout this Letter, we approximate the exponential growth rate as follows:

$$\frac{E'}{E} = \frac{d\log E(t)}{dt} \approx \frac{\log E(t + \Delta t) - \log E(t - \Delta t)}{2\Delta t}. \quad (1)$$

This approximation is used to mask the rapid fluctuation of the derivative. In some cases, again to suppress fluctuations, we may take E to be an average distance, averaging over several pairs of solutions.

We call an interval J of values of E a *log-linear regime,* if, for some $\lambda < 0$ and $C \leq E_s$ and all $E \in J$, E'/E approximately satisfies the linear differential equation [4]:

$$\frac{E'}{E} = \lambda \log(E/C). \quad (2)$$

The exponent λ describes how E approaches C. A typical dynamical system has one log-linear regime with $C = E_s$; then λ is called the *saturation exponent.* In this Letter, we investigate a realistic weather forecast model and find that this model has two distinct broad log-linear regimes (Fig. 1).

Weather model.—We are reporting a striking behavior for a global weather model, the National Centers for Environmental Prediction (NCEP) Global Forecast System (GFS). This formerly operational global atmospheric model is a pseudospectral model, described in detail in [5,6]. The resolution considered here is chosen such that it has a maximum zonal wave number of 62, and so is referred to as T62, where "T" stands for triangular truncation. There are 192×94 horizontal grid points at each of 28 vertical levels. In addition to the surface pressure, there are five variables defined at every grid point: (1) the vertical component of the vorticity of the horizontal wind, (2) the divergence of the horizontal wind, (3) a generalized temperature that reflects humidity, (4) the relative humidity, and (5) the ozone. Overall the state has dimension $N \approx 3 \times 10^6$.

We select a point $\mathbf{x}$ in the state space from a trajectory after transients have died away. We also choose at random

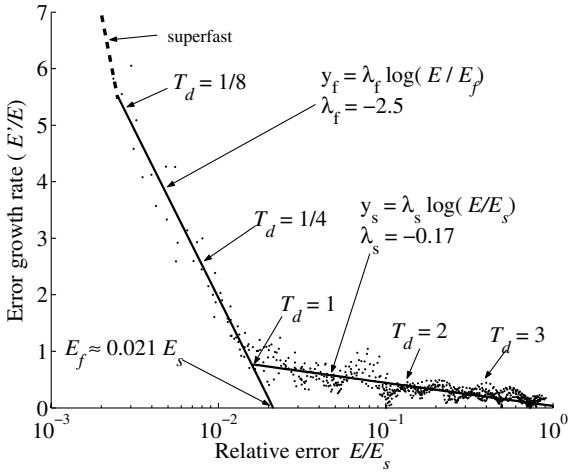

FIG. 1. Convex exponential error growth rate of the NCEP GFS model as a function of relative error E/E_s. The graph reveals two linear regimes. For $E < 0.02E_s$, E'/E lies close to line $y_f = \lambda_f \log(E/E_f)$ with $\lambda_f \approx -2.5$ and intercepts at $E_f \approx 2.1\%$ of the saturation level E_s. For $E > 0.02E_S$, E'/E lies close to the line $y_s = \lambda_s \log(E/E_s)$ with $\lambda_s \approx -0.17$. The doubling time of errors are 1/8, 1/4, 1, 2, and 3 days when E is 0.23%, 0.7%, 1.6%, 13%, and 26% of the saturation level, respectively. Small errors grow in amplitude, moving from left to right, first along the left line and then along the right until they saturate at E_s. Each point plotted here is for an individual pair of initial conditions. The dashes represent the "superfast" regime for $E < (2 \times 10^{-3})E_s$ (see text).

an N-vector $\delta\mathbf{p}$ and renormalize it so that $\| \delta\mathbf{p} \| = E_s$. We choose perturbed initial points

$$\mathbf{p}^k(0) = \mathbf{x}(0) + 10^{-k}\delta\mathbf{p} \quad \text{for } k = 3, \ldots, 7. \tag{3}$$

We do not show the cases for $k = 1, 2$ because we are interested in the behavior of perturbations that are initially small. Both the reference state $\mathbf{x}$ and perturbations $\mathbf{p}^k$ are integrated from $t = 0$ for 14 days with a 20 min time step. Now, define $E^k(t)$ to be the root-mean-square (rms) error of $\mathbf{x}$ and $\mathbf{p}^k$ for each k:

$$E^k(t) = \|\mathbf{p}^k(t) - \mathbf{x}(t)\|. \tag{4}$$

We focus our study on midlatitude tropospheric wind prediction. That is, calculations are restricted to the midlatitude bands in the Northern and Southern Hemispheres (22.5°–70° N/S) where the model is considered most accurate. We report the rms errors calculated for the atmospheric level where the pressure equals half of the surface pressure. We show only the rms errors of the vorticity, but the other variables behave in a similar way.

In Fig. 1, the exponential growth rate E'/E is plotted as a function of relative error size E/E_s in logarithmic coordinates. The error growth rate E'/E decays along two broad log-linear regimes (for time $t > 18$ h). In what we call the "fast regime" ($0.002E_s < E < 0.02E_s$), the errors double in less than a day. Here the error growth rates move along a straight line (2) with $\lambda = -2.5$ ($= \lambda_f$ in Fig. 1) as if to saturate at $C = E_f \approx 0.021E_s$, that is, 2.1% of the actual saturation size. After E reaches about $0.02E_s$, the growth rate enters the "slow regime." We refer to the point $E = 0.02E_s$ as the *KT boundary* [7]. After E passes the KT boundary, E'/E follows the straight line (2) with $\lambda = -0.17$ ($= \lambda_s$) and $C = E_s$. Here the growth rate E'/E slows to zero as E approaches its saturation level E_s. In creating Fig. 1, we approximate E'/E using (1) with $\Delta t = 6$ h, with t in steps of 3 h. The finite differences show some oscillation about the lines. We plot E'/E starting from $t = 18$ h because the NCEP model exhibits a third regime: superfast growth of extremely small perturbations. Errors of size less than $10^{-4}E_s$ climb rapidly to $10^{-4}E_s$, usually in about 1 h or less, even when beginning with size $10^{-7}E_s$ (not shown here). Thus, the errors grow to approximately $0.002E_s$ after 18 h independently of $E(0)$ provided $E(0) < 10^{-4}E_s$. Toth and Kalnay [8,9] investigated weather prediction using a reference state plus multiple perturbations as initial conditions. They report "enormous" growth of errors, more than a factor of 5 per day, when perturbations have an amplitude less than $0.001E_s$. They attribute such growth mostly to tropical convection, which they say saturates at less than $0.01E_s$. They see slow growth for amplitudes between $0.01E_s$ and $0.1E_s$ and attribute this behavior to baroclinic instabilities. They do not discuss the transition between these behaviors.

In contrast with the striking results of Fig. 1, simpler models often have a single log-linear regime. We illustrate the typical behavior of simpler models with the "Lorenz-40" model [1] of differential equations and the quasigeostrophic (QG) model of Marshall and Molteni [10] with resolution T21.

Lorenz-40 model.—The Lorenz-40 model [1,11] represents an "atmospheric variable" with values x_j at N equally spaced points around a circle of constant latitude:

$$5\frac{dx_j}{dt} = (x_{j+1} - x_{j-2})x_{j-1} - x_j + F, \tag{5}$$

where $j = 1, \ldots, N$ represent the spatial coordinates ("longitude"). Periodic boundary conditions are imposed by identifying $x_{-1} \equiv x_{N-1}$, $x_0 \equiv x_N$, and $x_{N+1} \equiv x_1$. This model is designed to satisfy three basic properties: it has linear dissipation (the $-x_j$ term) that decreases the total energy defined as $V = \frac{1}{2}\sum_{j=1}^{N} x_j^2$, an external forcing term F that can increase or decrease the total energy, and a quadratic advectionlike term that conserves the total energy (i.e., it does not contribute to $\frac{d}{dt}V$). Following [1,11], we choose the external forcing to be $F = 8$ and the number of spatial elements to be $N = 40$. The "5" in (5) scales the unit time to correspond to 1 day in real time. We also use a fourth-order Runge-Kutta scheme for time integration of (5) with time step $\Delta t = 1/4$ day. With these parameters, the solution to (5) has a behavior reminiscent of the midlatitude atmosphere. It has 13 positive Lyapunov expo-

nents, with the leading Lyapunov exponent corresponding to a doubling time of 2.1 days, and a Kaplan-Yorke dimension of 27.1 [1].

QG model.—The QG approximation describes weather-like slow atmospheric motion. Steady state flow in a rotating sphere satisfies the geostrophic balance; i.e., the horizontal pressure gradient balances the Coriolis force. Slow Rossby waves satisfy a quasigeostrophic balance as represented by the conservation of quasigeostrophic potential vorticity; see Holton [12]. In our study, we use the three-level QG model developed by Marshall and Molteni [10] with T21 resolution.

In the NCEP model, we examined the rms difference between a pair of trajectories $\mathbf{x}$ and $\mathbf{p}^k$. For the Lorenz-40 and QG models, we examine L such pairs of trajectories and average the resulting errors in order to mask the rapid fluctuation of E. The rms of the ith pair of $\mathbf{x}(t)$ and $\mathbf{p}^k(t)$ at time t, denoted as $E_i^k(t)$, is calculated from (4) for $i = 1, \ldots, L$. Then, we let $E^k(t)$ be the geometric mean

$$E^k(t) = \exp\langle \log E_i^k(t) \rangle, \tag{6}$$

where the average $\langle \cdots \rangle$ is computed over L pairs. Hence the previous $E^k(t)$ in Fig. 1 is an average of the $L = 1$ pair of trajectories. In contrast, we use $L = 1000$ for the Lorenz-40 model and $L = 100$ for the QG model. Both the reference state $\mathbf{x}$ and perturbations $\mathbf{p}^k$, with $k = 3, \ldots, 6$, are integrated with 6 h time steps from time $t = 0$ for 60 days for the Lorenz-40 model and for 360 days for the QG model.

In Figs. 2(a) for the Lorenz-40 model and 2(b) for the QG model, the exponential growth rates are plotted as functions of the relative rms difference between each $\mathbf{p}^k$ and $\mathbf{x}$. In creating these plots, the growth rate is approximated using (1) with $\Delta t = 1/2$ day for the Lorenz-40 model and $\Delta t = 10$ days for the QG model. Our experiments with the Lorenz-40 and the QG models show small averaged errors growing exponentially. Close to saturation (i.e., as $E \to E_s$), the exponential growth rate slows down as with differential Eq. (2) with $C = E_s$ and enters the log-linear regime. Specifically, the log-linear regime of the Lorenz-40 model is approximately $0.4E_s < E < E_s$ with saturation exponent $\lambda \approx -0.22$. We obtain a similar range of log-linear behavior with $\lambda \approx -0.035$ for the QG model. We believe that this single time scale behavior is due to the presence of only baroclinic instabilities in the QG model, while other instabilities (discussed at the end of this Letter) are present in the NCEP model. Next, we offer a scalar linear differential equation that justifies the typical error growth as observed in the Lorenz-40 or the QG model.

A simple error growth model.—Here we modify the logistic differential equation [13] and model the growth of the error $E(t)$ by a scalar differential equation:

$$E' = \frac{dE}{dt} = aE(1 - E^{-\lambda/a}). \tag{7}$$

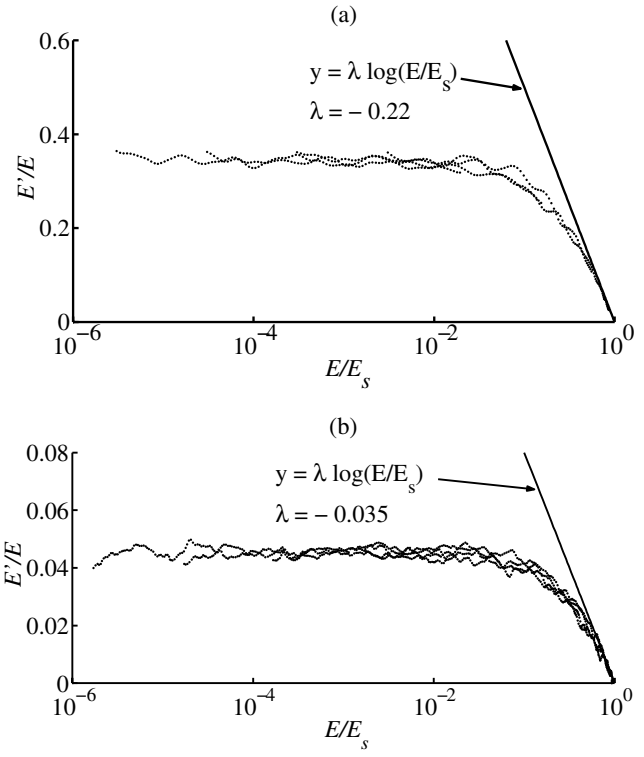

FIG. 2. Concave error growth rates, estimated by finite differences in (1), as functions of relative error E/E_s. (a) The error growth rate of the Lorenz-40 model fluctuates about 0.35 for $E < 10^{-3}E_s$ and decays in accordance to (2) where $\lambda = -0.22$ (see the line tangent to the growth rate) and $C = E_s$. (b) In the QG model, the growth rate fluctuates about 0.044 when $E < 10^{-3}E_s$ and decays asymptotically to (2) where $C = E_s$, with $\lambda = -0.035$ as $E > 0.4E_s$. As time increases, errors move from left to right, asymptoting to E_s. Each point plotted here is averaged over $L = 1000$ pairs of trajectories for the Lorenz-40 model and $L = 100$ for the QG model.

Near the steady state $E = 0$, we have $E'/E \approx a$. For $0 < E < 1$, we have $E \to 1$ as $t \to \infty$, and for $E \approx 1$, $E'/E \approx \lambda \log(E)$. With this variant of the logistic equation, two parameters, a and λ, can be selected independently. Figure 3 shows the exponential growth rate of the error, E'/E compared to E. We choose a and λ to fit the rate of the Lorenz-40 model in Fig. 2(a). For $E > 0.7$ [15], E'/E is close to the line (2) with $C = 1$. Similarly, the error growth rate of the QG model can be illustrated by (7) by choosing $a = 0.044$ and $\lambda = -0.035$.

Summary.—Convex error growth in the NCEP global atmospheric model contrasts with the concave error growth seen in simpler models that have a single type of instabilities. In the simple models we observe constant exponential growth that decreases once nonlinear effects become important. In the realistic weather model there is no exponential growth with constant E'/E. Instead, E'/E is strictly decreasing, indicating the presence of *multiple* types of instabilities that dominate at very different amplitude

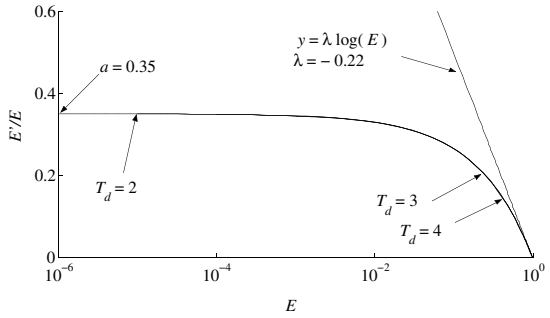

FIG. 3. Concave exponential growth rate, E'/E for (7) as a function of E in logarithmic scale. We set $a = 0.35$, $\lambda = -0.22$, $E(0) = 10^{-6}$, and $\Delta t = 1$. When $E < 10^{-3}$, we get $E'/E \approx a = 0.35$. As the error grows, the instantaneous doubling time T_d increases. We show $T_d = 2$, 3, and 4 corresponding to exponential growth rates of 0.34, 0.23, and 0.17, respectively. The line $y = \lambda \log(E)$ with $\lambda = -0.22$ is tangent to the E'/E curve at the asymptotic value $E = 1$.

ranges. We see an initial super rapid growth, followed by two log-linear regimes. This is reminiscent of the difference between the two-dimensional turbulence that dominates large scales (Charney [16]) and three-dimensional turbulence that dominates smaller scales, with a transition taking place for wavelengths between 400 and 1000 km (Nastrom and Gage [17], 1985). The shortest waves present in our model (with triangular truncation T62) have a wavelength of $40\,000\ \text{km}/62 \approx 320$ km so that there is only enough resolution to crudely resolve three-dimensional turbulent scales.

Our results suggest that the growth of perturbations occurs in three phases, and we examine the perturbation kinetic energy spectra (see Nastrom and Gage [17]) in each of these phases. In the first phase, tiny perturbations grow very fast through the most efficient mechanism that provides finite amplitude perturbation growth: the triggering of cumulus convection at slightly different times or locations. Because of the enormous latent heat energy released by convection, even the smallest perturbations that are computationally realizable become significant within an interval of a few convective time scales (within 1–3 h). In the first few time steps the perturbation kinetic energy is dominated by wave numbers larger than 32, corresponding to single grid point cumulus perturbations. After this initial supergrowth period, perturbations have acquired roughly the same finite size ($3 \times 10^{-3} E_s$) independent of the initial perturbations' sizes (Fig. 1). The fact that, during this period of superfast growth, ''butterfly''-sized model perturbations become significant supports the insight of Lorenz [2] and is consistent with the results of Zhang *et al.* [18] and Toth and Kalnay [8]. In the second phase, from 1–3 h to about 12–36 h, the perturbation spectrum shifts to waves between wave numbers 20 and 50 (wavelengths between 800 and 2000 km). This fast growth of small-scale perturbations is dominated by small-scale, turbulent dynamics. Beyond that time, the growth slows down further as the perturbation energy shifts to lower wave numbers in the range of two-dimensional turbulence, until by saturation time, the kinetic energy of the difference peaks at wave number 10 (about 4000 km, the characteristic wavelength of baroclinic instability).

While these results were obtained for the NCEP global model, we believe that they are relevant to all realistic models of the atmosphere that include convection.

The authors thank D. J. Patil and I. Szunyogh for many insightful discussions and criticisms. This research was partially supported by the NSF Grants No. DMS0104087 and No. ATM0328402, NOAA Grant No. NA040-AR4310103, NASA Grant No. NNG04GK78A, the Army Research Office, and the James S. McDonnell Foundation.

*Electronic address: jharlim@math.umd.edu
†Present address: Department of Physics and Astronomy, Francis Marion University, Florence, SC 29501.

[1] E. Lorenz, in *Proceedings of a Seminar held at ECMWF on Predictability, 1995* (European Centre for Medium-Range Weather Forecasts, Reading, U.K., 1996), pp. 1–18.
[2] E. Lorenz, Tellus **21**, 289 (1968).
[3] E. Aurell, G. Boffetta, A. Crisanti, G. Paladin, and A. Vulpiani, Phys. Rev. E **53**, 2337 (1996).
[4] All logs are natural logarithms; generally we want E'/E to be within 10% of $\lambda \log(E/C)$.
[5] J. Derber *et al.*, NOAA/NWS Technical Procedures Bulletin **449**, 16 (1998), available from Office of Meteorology, NWS, 1325 East-West Hwy., Silver Spring, MD 20910, USA.
[6] J. Sela, Monthly Weather Review **108**, 1279 (1980).
[7] Named after Toth and Kalnay [8,9] and the famous paleontological demarcation point.
[8] Z. Toth and E. Kalnay, Bull. Am. Meteorol. Soc. **74**, 2317 (1993).
[9] Z. Toth and E. Kalnay, Mon. Weather Rev. **125**, 3297 (1997).
[10] J. Marshall and F. Molteni, J. Atmos. Sci. **50**, 1792 (1993).
[11] E. Lorenz and K. Emmanuel, J. Atmos. Sci. **55**, 399 (1998).
[12] J. R. Holton, *An Introduction to Dynamic Meteorology* (Academic Press, New York, 1992), 3rd ed.
[13] Lorenz [14] modeled the error growth by the one-parameter logistic equation $E' = aE(1 - E)$. This equation, however, has an initial exponential growth rate equal to its saturation rate; that is, $a = -\lambda$ in (7). Such a constraint, as we see in Fig. 2, is not necessarily satisfied.
[14] E. Lorenz, Tellus **34**, 505 (1982).
[15] We say E is in the log-linear regime when $\frac{a(1-E^{-\lambda/a})}{\lambda \log E} > 0.9$, namely, for $E \in (0.7, 1)$.
[16] J. Charney, J. Atmos. Sci. **28**, 1087 (1971).
[17] G. Nastrom and K. Gage, J. Atmos. Sci. **42**, 950 (1985).
[18] F. Zhang, C. Snyder, and R. Rotunno, J. Atmos. Sci. **60**, 1173 (2003).